Investigation of subsonic jet noise using LES : Mach and Reynolds number effects.*

Christophe Bogey† and Christophe Bailly‡
Laboratoire de Mécanique des Fluides et d'Acoustique
Ecole Centrale de Lyon & UMR CNRS 5509
69134 Ecully, France.

Large Eddy Simulations (LES) of Mach number 0.6 and 0.9, circular jets with Reynolds numbers varying from 1.7×10^3 up to 4×10^5 are performed to investigate their radiated sound fields. As the Reynolds number decreases, the spectral properties of the sound radiation do not change significantly in the downstream direction, whereas they are basically modified in the sideline direction. For large angles from the jet axis, the acoustic levels are indeed significantly lower and a large high-frequency part of the sound spectra vanishes at low Reynolds numbers. Moreover, the noise spectra in both directions seem to scale with Strouhal number at any Reynolds number. The observations reported in the present paper also bring support to the presence of two components in subsonic jet noise: one, radiating downstream, associated to very large structures/instability waves, and an other connected to the fine-scale turbulence and therefore intrinsically dependent on the Reynolds number.

I. Introduction

The present paper is an effort to give new insights into subsonic jet noise using numerical simulations. After over fifty years of research indeed, whereas sound generation mechanisms in supersonic jets have been comprehensively described,[1] sound sources in subsonic jets are still to be clearly identified.[2] Two conflicting theories of jet noise have for instance been proposed by researchers. In the classical theory derived from the developments of acoustic analogies, the noise radiated by subsonic jets is generated by fine-scale turbulence and results from the complex combination of convective amplification and acoustic-meanflow interaction.[3] Unfortunately this view does not compound well with the experimental data suggesting that there are two distinguishable types of emitted sound.[4] Jet noise can thus be regarded as made of two basic components: one from the large structures/instability waves, dominating in the downstream direction, the other from the fine-scale turbulence, dominating in the sideline direction. This jet noise theory, strongly supported by works of Tam *et al.*[2,5] from a large database of sound spectra, is attractive. However it suffers, like others, from the confusing data available in the literature, whose trends can vary between experiments because of acoustic contamination[6] or of the use of one-third octave spectra.[7] Considering this, numerical simulations now offer an interesting tool for characterizing the properties of the jet sound field with accuracy, with the final aim of advancing the understanding of jet noise.

An important point to first address in the study of jet noise deals with the modifications of sound pressure spectra when jet parameters such as the Mach $M = u_j/c_0$ and the Reynolds number

†CNRS research scientist, christophe.bogey@ec-lyon.fr
‡Professor at Ecole Centrale de Lyon, Member AIAA, christophe.bailly@ec-lyon.fr

$\mathrm{Re}_D = u_j D/\nu$ are changed (u_j is the jet exit velocity, c_0 the speed of sound in the ambient medium, D the jet diameter, and ν the kinematic viscosity). For instance there is an enduring discussion about the scaling of the peak frequencies as the jet velocity varies. At high Reynolds numbers ($\mathrm{Re}_D \geq 10^5$), for an angle $\theta = 90^o$ from the jet axis, a Strouhal number $\mathrm{St} = fD/u_j$ scaling was found both from narrow-band[4] and one-third octave[8–10] spectra (f is the frequency). For shallow angles however, a Strouhal scaling was observed from narrow-band measurements[4] but an Helmholtz number $\mathrm{H} = fD/c_0$ scaling appeared from one-third octave spectra.[8–10] Zaman & Yu[7] later shown that this Helmholtz scaling is an artifact of the use of one-third octave, resulting in a shift of the peak frequency, and found that the best scaling for shallow angles is obtained with the Helmholtz number times a Doppler factor, *i.e.* with $\mathrm{H}(1 - 0.5\mathrm{M}\cos\theta)$. The preceding observations have been made at high Reynolds numbers, but are likely not to apply at low Reynolds numbers since jet noise sources may be modified below $\mathrm{Re}_D \simeq 10^5$, as noticed by Crighton[11] from sound radiation of excited jets. At low Reynolds numbers[12,13] indeed, the properties of jet noise change significanly, with much narrower spectra and lower pressure levels at large observation angles. These changes may naturally result from the reduction of fine-scale turbulence with decreasing Re_D. More surprisingly, Long & Arndt[13] found an Helmholtz scaling for the peak frequencies at all angles, which has to be carefully checked. Note finally that the study of low Reynolds number jets can be particularly useful for the investigation of the sound sources attributed to large turbulent structures. Simulations of jets at low Reynolds number have thus allowed to connect the downstream sound radiation to the instability waves in the shear layer[14] or to the periodic intrusion of vortical structures in the jet[15] at the end of the potential core.

In the present work, Large Eddy Simulations (LES) of circular jets at Mach numbers $\mathrm{M} = 0.6$ and 0.9, with Reynolds numbers Re_D varying from 1700 up to 4×10^5 are performed to compare their respective acoustic radiations, and thus bring informations on sound sources. This is the continuation of earlier studies where Mach $\mathrm{M} = 0.9$ jets at Reynolds number $\mathrm{Re}_D = 4 \times 10^5$ have been simulated. In these studies, flow and sound properties[16] in agreement with what is expected at this high Re_D have been obtained, and the influence of the inflow conditions[17] and of the subgrid modelling[18] on results have then been investigated. Remind that unlike Direct Numerical Simulation (DNS), LES can be applied to any Reynolds number provided that the LES methodology preserves the effective Re_D given by the jet initial conditions. Present simulations are thus performed using a solver developed for direct noise computations with low-dissipative and low-dispersive numerical schemes,[19] following an LES approach based on an explicit selective filtering instead of a classical eddy-viscosity model for subgrid modelling.[16,20] For the simulated jets, the properties of the sound pressure field are investigated at two observation points located at $x = 29r_0$ and $r = 12r_0$, and at $x = 11r_0$ and $r = 15r_0$, respectively (r_0 is the jet radius). The effects of Mach and Reynolds numbers on the downstream and sideline acoustic radiations are thus shown. Attention is especially turned to the alterations made to the sound spectra and azimuthal cross-correlations, and to the scaling of the peak frequencies and levels. In this way, the presence and the characteristics of the two possible noise sources in subsonic jets can be examined.

The paper is organized as follows. In section II, the main features of the numerical procedure are presented and the different simulations are defined. The sound pressure fields radiated by the simulated jets are investigated in section III: snapshots of vorticity and pressure are displayed, and properties of the sound fields in the downstream and sideline directions are compared. Jet noise sources are discussed in the light of the numerical results in section IV. Finally concluding remarks are drawn in section V.

II. Simulation parameters

A. Numerical procedure

The numerical algorithm is identical to that of the earlier simulation[16] of a Mach $\mathrm{M} = 0.9$, Reynolds $\mathrm{Re}_D = 4 \times 10^5$ jet. The filtered compressible Navier-Stokes equations are solved using highly accurate numerical schemes with low dispersion and low dissipation properties.[19] A thirteen-point finite-difference scheme is used for spatial discretization while an explicit six-stage Runge-Kutta algorithm is applied for time integration. Grid-to-grid oscillations are removed thanks to an explicit filtering which is optimized to damp only the short waves discretized by less than four points per wavelength.

It is used to ensure numerical stability, and also to take into account the effects of the subgrid energy-dissipating scales without affecting the resolved scales. This approach was developed to preserve the effective Reynolds number of the jet, which might not be possible using eddy-viscosity subgrid models such as the dynamical Smagorinsky model.[18] Moreover to directly compute the noise, non-reflective boundary conditions are implemented, with the addition of a sponge zone at the outflow.[21]

The numerical parameters of the present simulations are those of the simulation referred to as LESac or LESsf in earlier papers.[16–18] The computational domain is discretized by a 12.5 million point Cartesian grid with 15 points in the jet radius r_0. The flow is computed up to an axial distance of $x = 25r_0$. The sound field is calculated up to $x = 30r_0$ and, radially, up to $r = 15r_0$ from the jet axis, and resolved for Strouhal numbers $St = fD/u_j < 2$. Finally, the simulation times T are long enough to achieve convergence of statistics, as indicated for instance by the corresponding Strouhal number $D/(Tu_j) \simeq 10^{-3}$.

B. Definition of the simulations

Initial conditions are defined for eight isothermal round jets with centerline velocities and diameters yielding Mach numbers M of 0.6 and 0.9 and Reynolds numbers Re_D varying from 1700 up to 4×10^5. They are given in Table 1. The LESac simulation is the jet simulation at Mach M = 0.9 and at the high Reynolds number $\mathrm{Re}_D = 4 \times 10^5$ referred also to as LESac[16,17] or as LESsf[18] in earlier papers. In the LESre1, LESre2, LESre3 and LESre4 simulations, the Mach number remains M = 0.9 but the Reynolds number is progressively decreased down to a value of $\mathrm{Re}_D = 1700$. In the LESmach1, LESmach2 and LESmach3 simulations, the Mach number is M = 0.6 only, the first simulation being at high Reynolds number whereas the two others are at low Reynolds numbers. A graph of the jet initial conditions is provided in Figure 1; note that the LESre4 and the LESmach3 simulations are both at $\mathrm{Re}_D = 1700$.

	M	Re_D
LESac	0.9	4×10^5
LESre1	0.9	10^4
LESre2	0.9	5×10^3
LESre3	0.9	2.5×10^3
LESre4	0.9	1.7×10^3
LESmach1	0.6	2.7×10^5
LESmach2	0.6	3.3×10^3
LESmach3	0.6	1.7×10^3

Table 1: Mach and Reynolds numbers of the simulated jets.

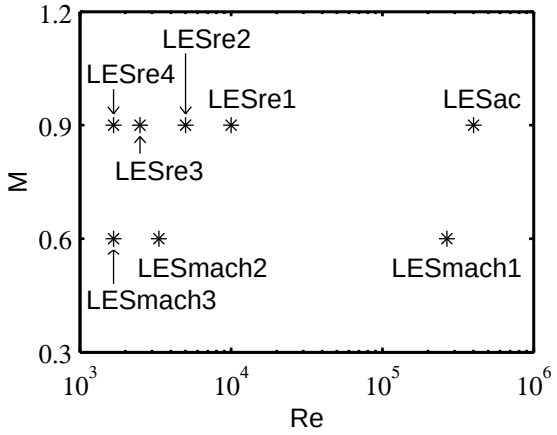

Figure 1: Graph of the initial conditions of the simulated jets.

In all simulations, mean profiles of velocities, pressure and density are imposed at the jet inflow

boundary. The axial velocity is given by a hyperbolic-tangent profile describing an annular shear layer of radius r_0 and of momentum thickness δ_θ, with a ratio $\delta_\theta/r_0 = 0.05$. Radial and azimuthal velocities are set to zero, pressure is set to the ambient pressure, and the mean density profile is obtained from a Crocco-Buseman relation. To seed the turbulence, small random disturbances are added to the velocity profiles in the shear layer zone following the procedure used in the LESac simulation. This procedure is reported in detail in a recent paper[17] where the effects of the inflow conditions on flow and sound fields are studied.

Finally profiles will be plotted in the next section to compare the sound field properties. They will follow the line type definitions of Table 2 for the Mach 0.9 jets, and those of Table 3 for the Mach 0.6 jets.

LESac	———
LESre1	– – –
LESre2	– · – ·
LESre3	·····
LESre4	oooooo

Table 2: Line types used for the comparisons of the Mach 0.9 jet results.

LESmach1	———
LESmach2	– – –
LESmach3	·····

Table 3: Line types used for the comparisons of the Mach 0.6 jet results.

III. Results

A. Instantaneous vorticity and pressure

Snapshots of the vorticity norm and of the fluctuating pressure are presented in Figure 2 for the simulations LESac, LESre2, LESre3 and LESre4 at Mach 0.9 and in Figure 3 for the simulations LESmach1 and LESmach3 at Mach 0.6. As the Reynolds number decreases, the jet flow changes significantly. At high Reynolds number in LESac and LESmach1, the turbulent flow field shows a large range of vortical scales, whereas at low Reynolds number, for instance in LESre4 at $\mathrm{Re}_D = 1700$, a large part of the fine scales disappears due to molecular viscosity. At low Reynolds number, viscosity also appears to notably affect the shear-layer development. As seen in LESre4, the shear-layer thickness increases by viscous diffusion, and the generation of vortical structures in the shear layer occurs later. This must be related to the decrease of the growth rates of instability waves.[22] Another observation can be made at the very low Reynolds number in LESre4: coherent turbulent structures appear in the shear layer close to the end of the potential core, displaying a length scale comparable with the jet radius, which may prevent vortex pairings. The differences of jet developments according to Mach and Reynolds numbers are also illustrated by the core lengths x_c determined here from the centerline mean axial velocity u_c using $u_c(x_c) = 0.95u_j$, and given in Table 4 for the high and lower Reynolds number jets. The core length is found to be about $10r_0$ at high Re_D but about $14r_0$ at $\mathrm{Re}_D = 1700$. Moreover, the potential core is shorter as the Mach number decreases, in agreement with experimental observations[23] and with the linear instability theory.[22]

LESac	$x_c = 10.2r_0$
LESmach1	$x_c = 9.5r_0$
LESre4	$x_c = 15.9r_0$
LESmach3	$x_c = 13.3r_0$

Table 4: Core lengths obtained for the high Reynolds (top) and the $\mathrm{Re}_D = 1700$ (bottom) jets.

The snapshots of Figures 2 and 3 also show the important alterations of the radiated pressure field as the Mach and Reynolds numbers vary. First, the acoustic wavelengths are clearly found to increase

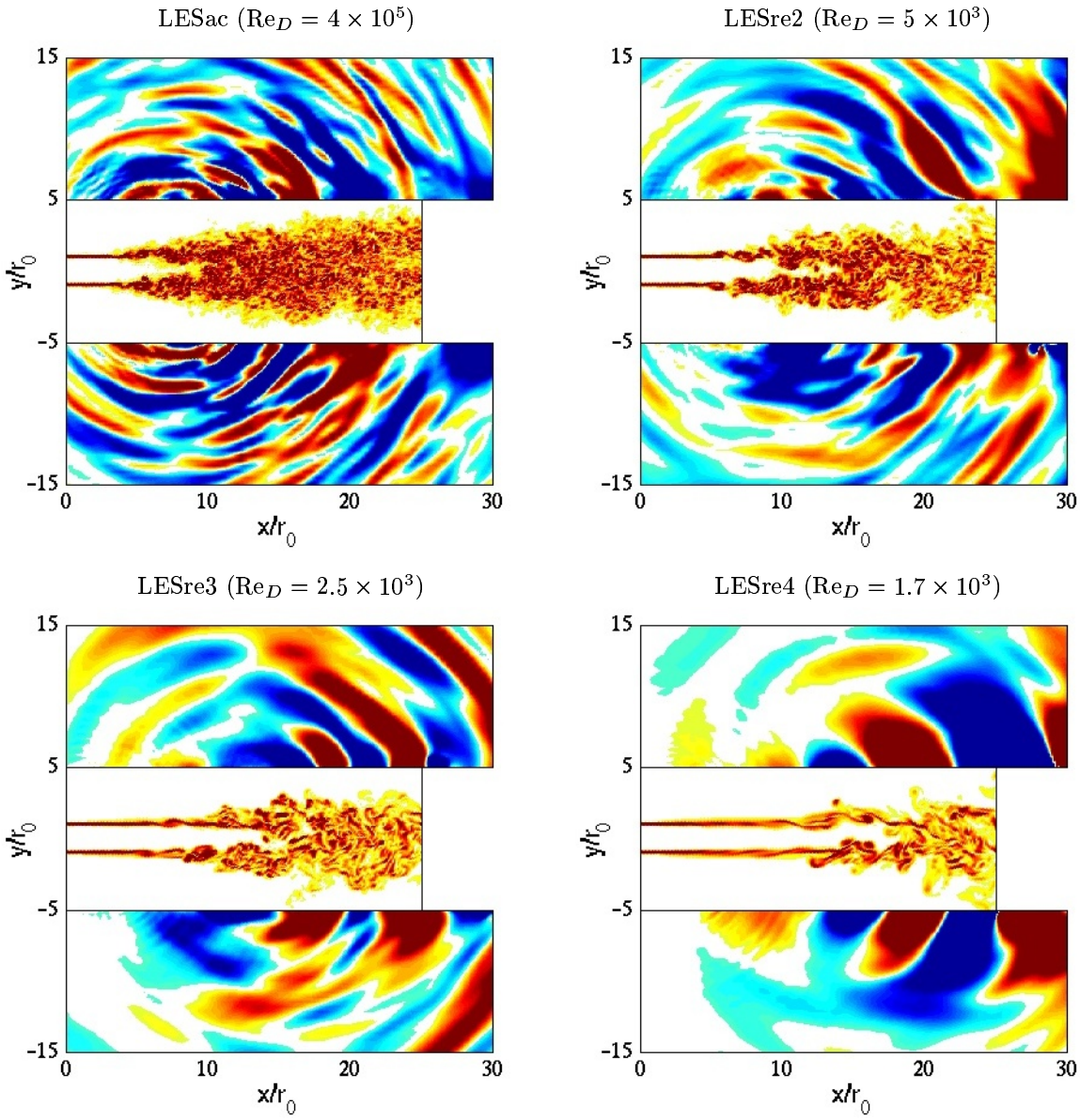

Figure 2: Jets at Mach M = 0.9. Snapshots of the vorticity norm in the flow and of the fluctuating pressure outside, in the plane $z = 0$. The vorticity color scales are $[0, 8\times10^4]$ s^{-1} for LESac, $80\times[0, 8\times10^4]$ s^{-1} for LESre2, $160\times[0, 8\times10^4]$ s^{-1} for LESre3, and $240\times[0, 8\times10^4]$ s^{-1} for LESre4. The pressure color scale is $[-70, 70]$ Pa for the four simulations.

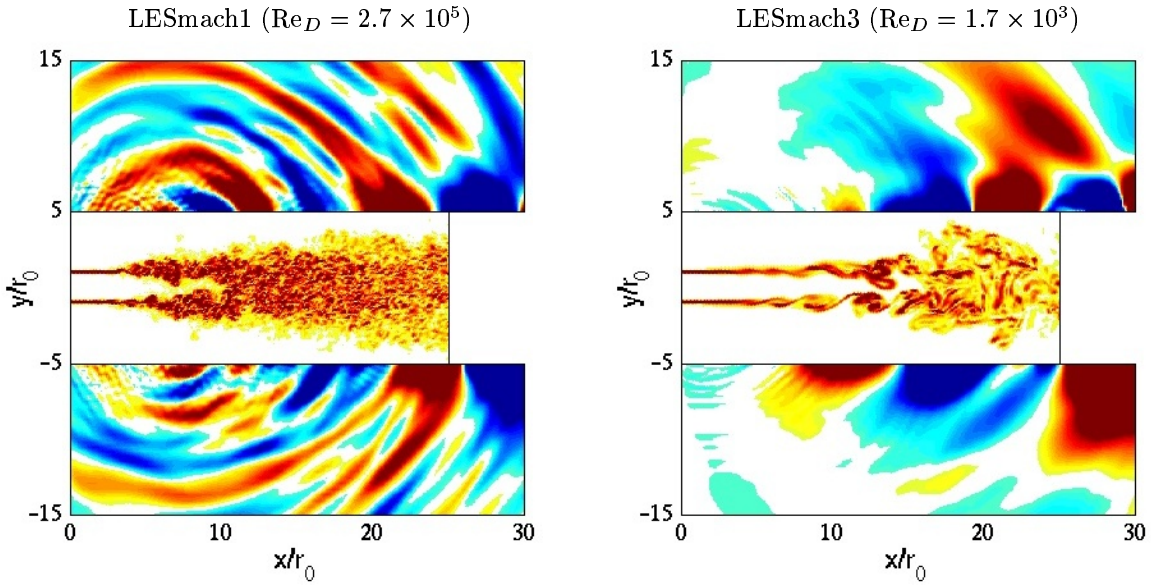

Figure 3: Jets at Mach M = 0.6. Snapshots of vorticity and of pressure at $z = 0$. The vorticity color scales are $[0, 6{\times}10^4]$ s^{-1} for LESmach1, and $160{\times}[0, 6{\times}10^4]$ s^{-1} for LESmach3. The pressure color scale is $[-20, 20]$ Pa for both simulations.

when the Mach number is lowered, as expected, see for instance the sound fields obtained from the two high Reynolds number simulations LESac and LESmach1. Second, as for the turbulent field, the high-frequency sound waves appear to progressively vanish as the Reynolds number is decreased. Compare for instance the sound fields obtained at high Re_D in LESac and at $\mathrm{Re}_D = 1700$ in LESre4: short waves are well visible in LESac whereas only low-frequency waves remain in LESre4. Moreover, the disappearance of short waves at low Re_D visibly leads to a significant reduction of the sound levels for large radiation angles from the downstream direction.

The modifications of radiation magnitude are shown more quantitatively in Figure 4 by the sound pressure levels obtained at $r = 15r_0$ for the Mach 0.9 and Mach 0.6 jets. At varying Reynolds numbers, sound levels are similar at $x \simeq 30r_0$, *i.e.* for emission angles $\theta \simeq 40^o$, but quite scattered at $x \leq 20r_0$ for larger angles. A reduction of about 6 dB is noticed at $x \simeq 10r_0$, in the direction perpendicular to the jet axis, between simulations at high Re_D and at $\mathrm{Re}_D = 1700$. These changes are in good agreement with experimental data.[12]

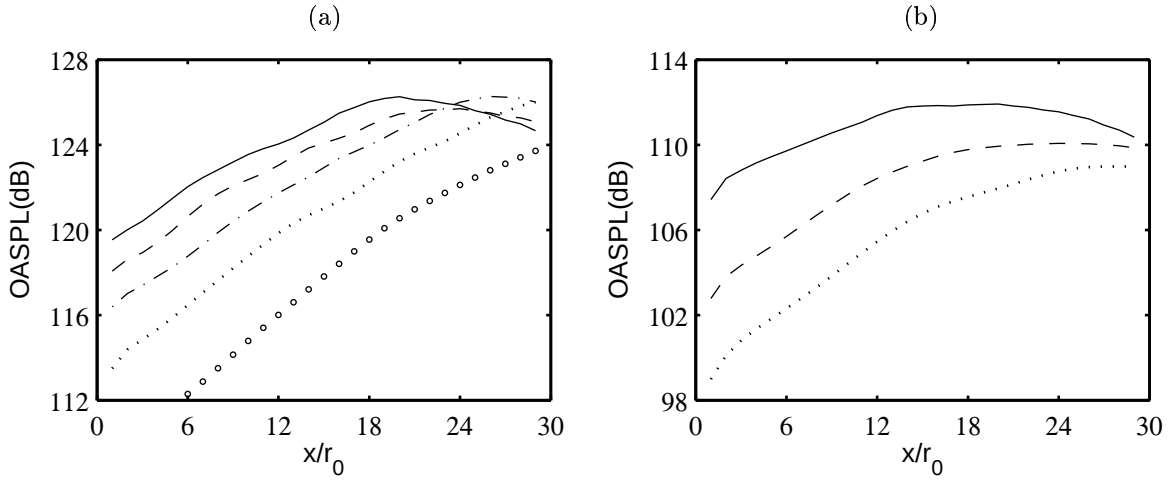

Figure 4: Overall sound pressure levels at $r = 15r_0$: (a) Mach 0.9 jets, see Table 2 for the line types; (b) Mach 0.6 jets, see Table 3.

B. Downstream sound field

Properties of the downstream sound field are now investigated at the observation point located at $x = 29r_0$ and $r = 12r_0$. The radiation angle from the jet direction is here about $\theta = 30^o$.

1. Sound spectra

The sound spectra calculated at the downstream observation point are presented in Figure 5(a) and (b) for the Mach 0.9 and Mach 0.6 jets, in linear scales, as a function of Strouhal number. Their shapes appear to moderately change with the Reynolds number. All spectra are dominated by a low-frequency component at Strouhal St $\simeq 0.25$, which however seems more pronounced at low Reynolds number. Moreover, for both Mach numbers, the peak level is found to be enhanced as the Reynolds number decreases, down to a threshold value $\mathrm{Re}_D \simeq 2000$ below which it is then lowered. Its maximum increase with respect to the high Re_D case is only about 2 dB.

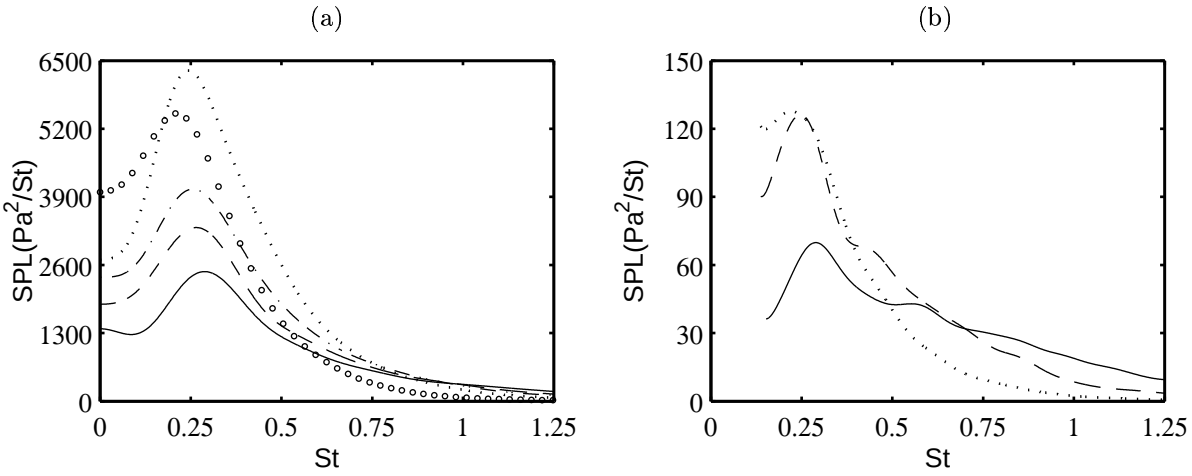

Figure 5: Downstream pressure spectra at $x = 29r_0$ and $r = 12r_0$, as a function of Strouhal number $\mathrm{St} = fD/u_j$: (a) Mach 0.9 jets, see Table 2 for the line types; (b) Mach 0.6 jets, see Table 3.

To evaluate the variations of sound spectra with velocity, the spectra obtained at similar Reynolds numbers are depicted in Figure 6, in logarithmic scales, using different scaling factors to correct the sound levels of the Mach 0.6 jets.

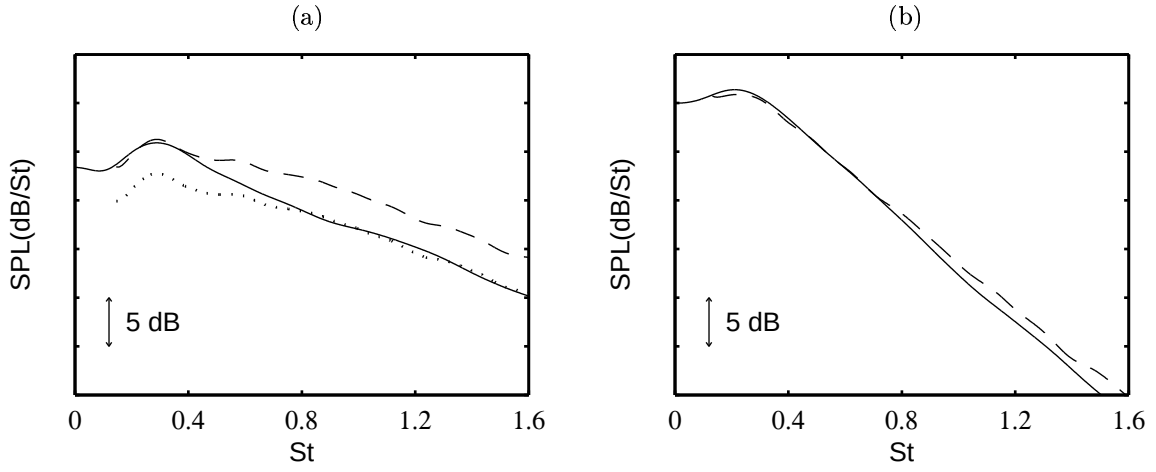

Figure 6: Pressure spectra obtained at $x = 29r_0$ and $r = 12r_0$ for: (a) the high Reynolds number jets, (b) the $\mathrm{Re}_D = 1700$ jets. Levels: ——— at Mach $\mathrm{M}_h = 0.9$; – – – at Mach $\mathrm{M}_l = 0.6$, multiplied by a $(\mathrm{M}_h/\mathrm{M}_l)^9$ scaling factor; ····· at $\mathrm{M}_l = 0.6$, multiplied by $(\mathrm{M}_h/\mathrm{M}_l)^7$.

At high Reynolds number in Figure 6(a), the peak levels are thus shown to vary as u_j^9 whereas

the high-frequency parts of the spectra for St ≥ 0.8 collapse successfully following a u_j^7 scaling. These results agree with the corresponding experimental far-field observations at $\theta = 30°$. Zaman & Yu[7] noticed for instance a $u_j^{9.5}$ variation of the peak level while the high-frequency levels were seen to increase at a lower exponent.[4,7] However this difference of variations between low and high frequency levels does not seem to exist for the $\mathrm{Re}_D = 1700$ spectra in Figure 6(b). In this case, the power law of u_j^9 applies fairly well not only for the peak but also for the whole frequency range. Finally note the different decreases of the sound levels towards high Strouhal numbers according to Reynolds number: the gap between the peak and the St = 1.5 levels is about 15 dB at high Re_D, but about 30 dB at $\mathrm{Re}_D = 1700$.

The peak frequencies are now represented as a function of Reynolds number. As shown in Figure 7(a), they collapse well using Strouhal number scaling. The peak Strouhal number is found to slightly decrease at lower Reynolds numbers, with for instance $\mathrm{St}_{peak} = 0.28$ at high Re_D versus $\mathrm{St}_{peak} = 0.22$ at $\mathrm{Re}_D = 1700$. Moreover, Helmholtz number scaling is displayed in Figure 7(b), and it is clearly seen to be unappropriate.

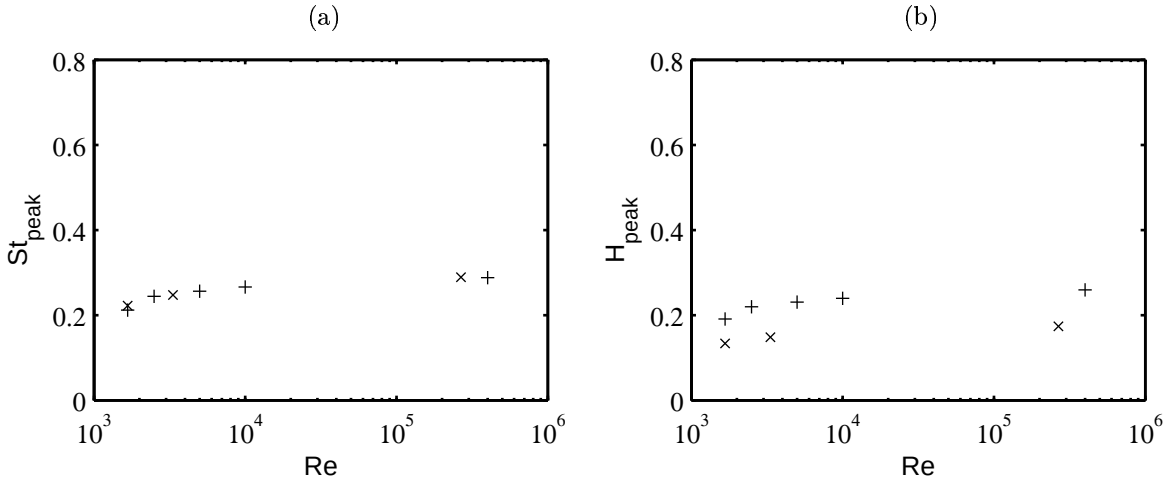

Figure 7: Scaling with Reynolds number of the pressure spectrum peaks obtained at $x = 29r_0$ and $r = 12r_0$ for jets at: + Mach 0.9; × Mach 0.6. (a) peak Strouhal numbers $\mathrm{St}_{peak} = f_{peak}D/u_j$; (b) peak Helmholtz numbers $\mathrm{H}_{peak} = f_{peak}D/c_0$.

For completeness, the scaling with the Helmholtz number times the Doppler factor $(1 - \mathrm{Mc}\cos\theta)$, where Mc is assumed to be the source convection Mach number, is tested in Figure 8.

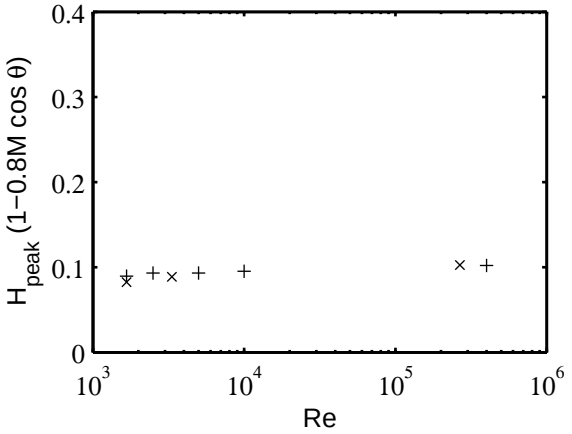

Figure 8: Scaling with Reynolds number of the pressure spectrum peaks $\mathrm{H}_{peak}(1 - 0.8\mathrm{M}\cos\theta)$ obtained at $x = 29r_0$ and $r = 12r_0$. See caption of Figure 7 for the symbols.

Zaman & Yu[7] observed that the best collapse of the spectra for shallow angles is yielded for

Mc = 0.5M. In the present work, with θ calculated from the end of the potential core x_c, the best scaling, shown in Figure 8, is obtained for Mc = 0.8M. From the numerical results, it is therefore difficult to settle the matter of scalings with Strouhal versus with Helmholtz times a Doppler factor for the downstream sound spectra. The latter scaling may however depend on the choice of the parameter Mc, and still needs physical justifications not to appear only as an *ad hoc* scaling.

2. Azimuthal correlations

To study the structure of the downstream sound field, the azimuthal cross-correlation functions of the fluctuating pressure are calculated at the observation location at $x = 29r_0$ and $r = 12r_0$. They are presented in Figure 9(a) for the Mach 0.9 jets and in Figure 9(b) for the Mach 0.6 jets, and display high correlation levels as expected for shallow angles.[24] These levels are very similar at $\mathrm{Re}_D \geq 5000$, but they appear to somewhat decrease at lower Reynolds numbers. For instance the correlation level for the azimuthal angle $\phi = 180^o$ is about 0.5 at high Re_D, but only about 0.3 at $\mathrm{Re}_D = 1700$.

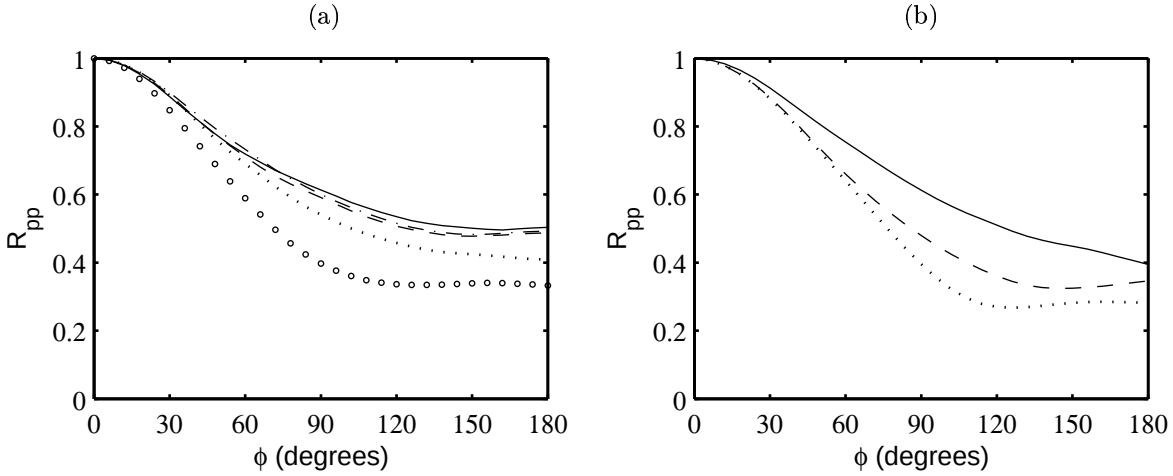

Figure 9: Azimuthal cross-correlations of the fluctuating pressure at $x = 29r_0$ and $r = 12r_0$: (a) Mach 0.9 jets, see Table 2 for the line types; (b) Mach 0.6 jets, see Table 3.

The correlation functions are now displayed in Figure 10(a) for the high Reynolds jets and in Figure 10(b) for the $\mathrm{Re}_D = 1700$ jets. In both cases, the correlation obtained at Mach 0.6 is slightly higher for $\phi \leq 90^o$ but lower for $\phi \geq 90^o$ compared to that obtained at Mach 0.9. This trend as the velocity varies corresponds well with far-field measurements[24] at $\theta = 30^o$.

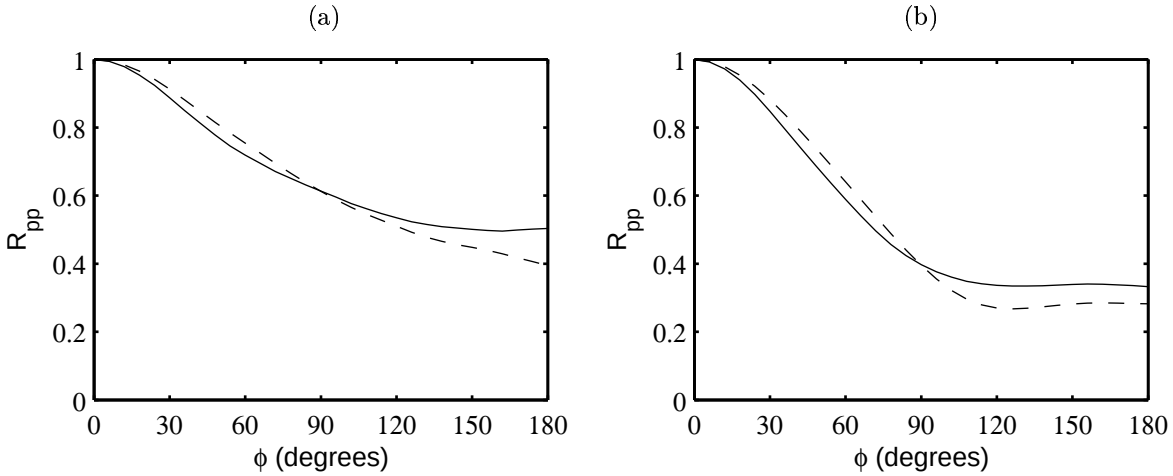

Figure 10: Azimuthal cross-correlations of the fluctuating pressure obtained at $x = 29r_0$ and $r = 12r_0$ for : (a) the high Reynolds number jets, (b) the $\mathrm{Re}_D = 1700$ jets; at : ——— Mach 0.9, – – – Mach 0.6.

Finally the modal contribution to the downstream sound field is provided in Table 5 for the high Re_D and the $\mathrm{Re}_D = 1700$ jets. It is shown to be nearly unaffected by changes in Mach or Reynolds numbers, even if the mode $m = 0$ appears to be rather enhanced at high Reynolds. In all cases, the mode $m = 0$ is dominant with about 70% of the total sound field whereas the mode $m = 1$ contains about 25% of the acoustic field, which agrees with experimental data[25] at $\theta = 30^o$.

	$m = 0$	$m = 1$	$m = 2$
LESac	0.73	0.25	0.02
LESmach1	0.74	0.25	0.02
LESre4	0.69	0.27	0.03
LESmach3	0.69	0.28	0.03

Table 5: Contributions to the acoustic field at $x = 29r_0$ and $r = 12r_0$ of the first three azimuthal modes for the high Reynolds (top) and the $\mathrm{Re}_D = 1700$ (bottom) jets.

C. Sideline sound field

The computed sideline sound fields are now investigated at an observation point perpendicular to the end of the potential core, at $x = 11r_0$ and $r = 15r_0$.

1. Sound spectra

The sound spectra calculated at the study point are presented in Figure 11(a) and (b) for the Mach 0.9 and the Mach 0.6 jets, in linear scales, as a function of Strouhal number. As the Reynolds number decreases, they change spectacularly with the disappearance of the high-frequency components, as expected.[13] Moreover the lower the Reynolds number, the larger the part of the spectra vanished. As a consequence the peak frequency progressively moves to lower Strouhal numbers, with for instance for the Mach 0.9 jet $\mathrm{St}_{peak} \simeq 0.7$ at high Reynolds number but only $\mathrm{St}_{peak} \simeq 0.2$ at $\mathrm{Re}_D = 1700$. For these two jets, note also the significant reduction in spectral band-widths: about $0 \leq \mathrm{St} \leq 1.5$ versus $0 \leq \mathrm{St} \leq 0.4$.

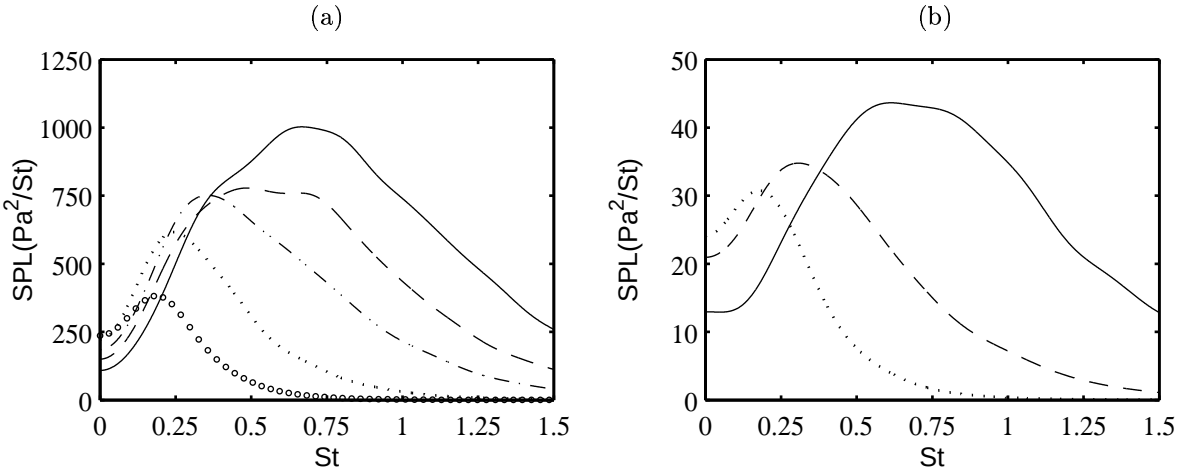

Figure 11: Sideline pressure spectra at $x = 11r_0$ and $r = 15r_0$, as a function of Strouhal number $\mathrm{St} = fD/u_j$: (a) Mach 0.9 jets, see Table 2 for the line types; (b) Mach 0.6 jets, see Table 3.

The variations with velocity of the sideline sound spectra are shown in Figure 12 where the spectra obtained at high Reynolds number are depicted in logarithmic scales. The spectra of the Mach 0.6 and Mach 0.9 jets collapse very well over the whole frequency range using a $u_j^{7.5}$ scaling to adjust the levels of the lower Mach number jet. This $u_j^{7.5}$ power law is exactly that determined by Zaman & Yu[7] from experimental far-field spectra at $\theta = 90^o$.

Strouhal number and Helmholtz number peaks are now represented in Figure 13 as a function of Reynolds number. The Strouhal number scaling appears to apply at high Reynolds number, as

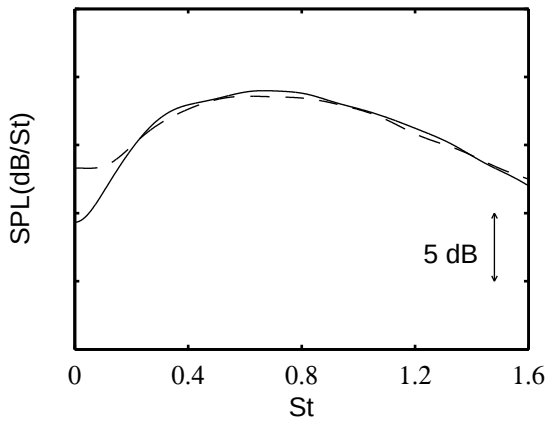

Figure 12: Pressure spectra obtained at $x = 11r_0$ and $r = 15r_0$ for the high Reynolds number jets. Levels : ——— at Mach $M_h = 0.9$; − − − at Mach $M_l = 0.6$, multiplied by a $(M_h/M_l)^{7.5}$ scaling factor.

found experimentally,[4] but also at low Reynolds number. As a result the Helmholtz scaling is not appropriate, even at low Reynolds number as clearly shown with the results at $Re_D = 1700$. This latter point is at variance with the experimental data of Long & Arndt[13] who gave evidence of Helmholtz scaling at low Re_D for the angle $\theta = 90^o$.

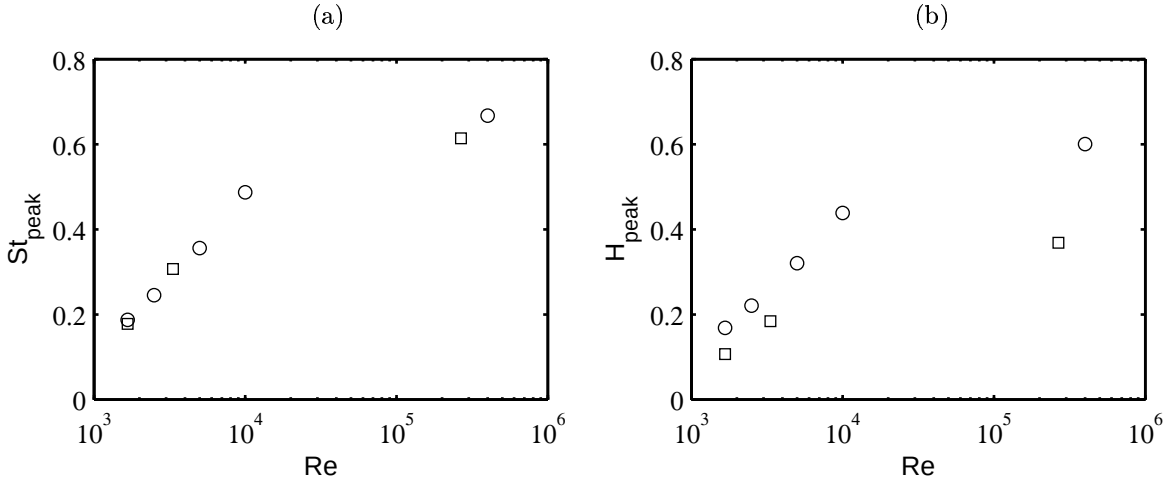

Figure 13: Scaling with Reynolds number of the pressure spectrum peaks obtained at $x = 11r_0$ and $r = 15r_0$ for jets at: o Mach 0.9; □ Mach 0.6. (a) peak Strouhal numbers $St_{peak} = f_{peak}D/u_j$; (b) peak Helmholtz numbers $H_{peak} = f_{peak}D/c_0$.

2. Azimuthal correlations

The azimuthal cross-correlation functions of the sound field at the study location are presented in Figure 14(a) for the Mach 0.9 jets and in Figure 14(b) for the Mach 0.6 jets. They show low correlation levels, in agreement with experimental observations for large angles.[24] The correlation is enhanced as the Reynolds number decreases, especially for large azimuthal angles as illustrated by the correlation obtained at $\phi = 180^o$ for the Mach 0.6 jet (nearly 0 at high Reynolds number versus 0.4 at $Re_D = 1.7 \times 10^3$).

The cross-correlation functions obtained in the sideline direction are now represented in Figure 15(a) for the high Reynolds jets and in Figure 15(b) for the $Re_D = 1700$ jets. At high Reynolds number, the correlations determined at Mach 0.6 and Mach 0.9 do not significantly differ for any azimuth. At the low Reynolds number, the correlations are also very similar except for large azimuthal angles $\phi \simeq 180^o$ where the correlation is higher at the lower Mach number as found experimentally[26] in far field at $\theta = 90^o$.

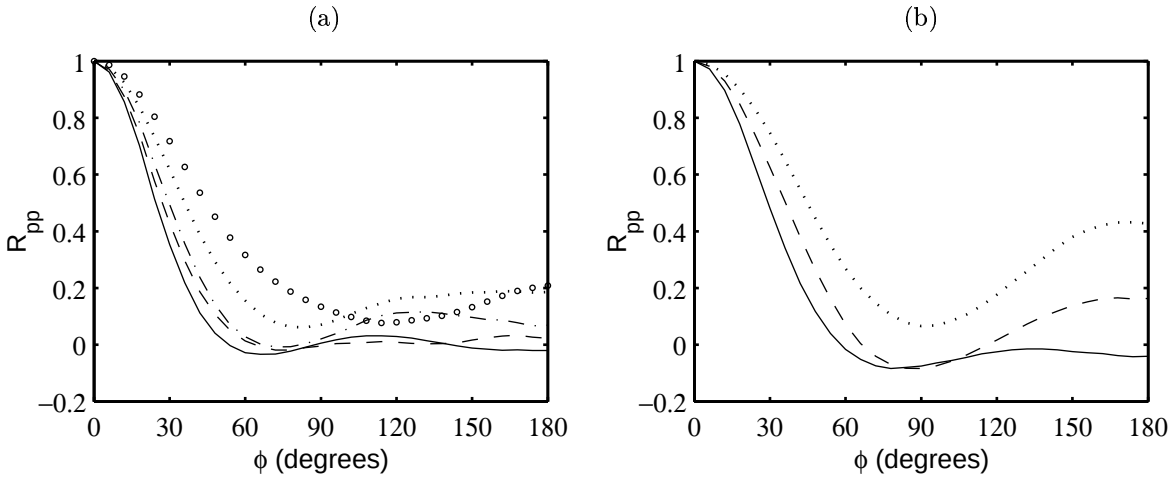

Figure 14: Azimuthal cross-correlations of the fluctuating pressure at $x = 11r_0$ and $r = 15r_0$: (a) Mach 0.9 jets, see Table 2 for the line types; (b) Mach 0.6 jets, see Table 3.

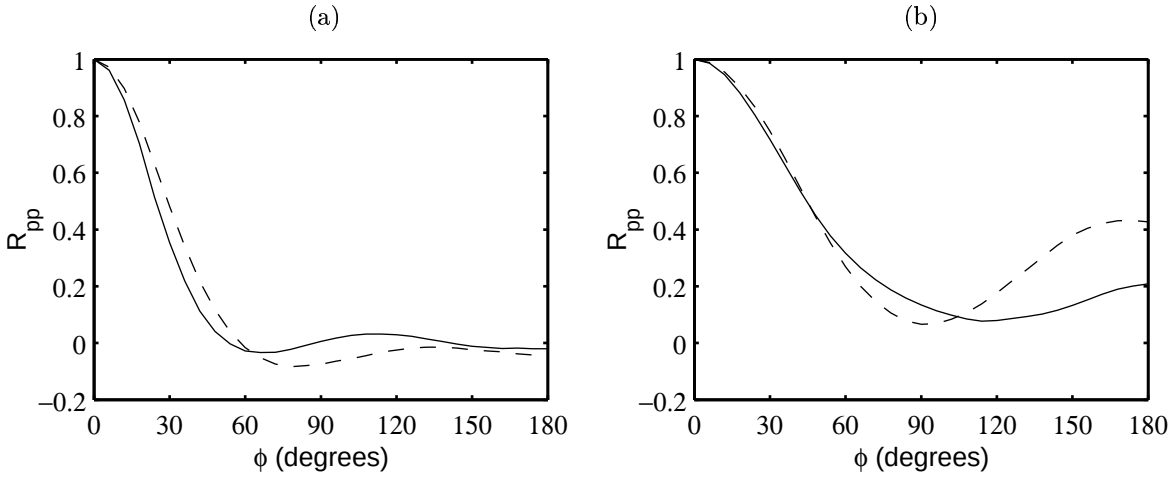

Figure 15: Azimuthal cross-correlations of the fluctuating pressure obtained at $x = 11r_0$ and $r = 15r_0$ for : (a) the high Reynolds number jets, (b) the $\mathrm{Re}_D = 1700$ jets; at : ——— Mach 0.9, – – – Mach 0.6.

	$m = 0$	$m = 1$	$m = 2$	$m = 3$
LESac	0.43	0.34	0.17	0.05
LESmach1	0.47	0.36	0.14	0.02
LESre4	0.60	0.33	0.06	0.01
LESmach3	0.60	0.33	0.06	0.01

Table 6: Contributions to the acoustic field at $x = 11r_0$ and $r = 15r_0$ of the first four azimuthal modes for the high Reynolds (top) and the $\mathrm{Re}_D = 1700$ (bottom) jets.

The modal contribution to the sideline acoustic field is finally reported in Table 6 for the high Re_D and the $\mathrm{Re}_D = 1700$ jets. It is first shown to depend on the Mach number very weakly. Second, as the Reynolds number decreases, the dominance of the mode $m = 0$ is enhanced while the contribution of the mode $m = 2$ is notably reduced. With respect to the modal contribution to the downstream sound field, the modes $m = 1$ and $m = 2$ here contain a great part of the total field, even if the mode $m = 2$ is here not dominant which is in disagreement with some far-field experiments[25] at $\theta = 90^o$.

IV. Discussion on sound sources

The modifications of the sound field obtained in the present simulations at the downstream and sideline observation points as the Mach and Reynolds numbers vary bring support to the theory of two sound sources in subsonic jets. They provide also informations about features of the radiations generated by these two basic sources.

There appears to be a first sound source responsible for a radiation whose properties are closely dependent on the Reynolds number. This radiation dominates in the sideline direction for the whole frequency range of spectra. It seems to be also observed in downstream spectra for high frequencies, but at high Reynolds numbers only as suggested by the level scalings in Figure 6. At a given Reynolds number, the variations with the velocity of its associated spectral components follow a Strouhal number scaling and a power law of $u_j^{7.5}$ or u_j^7, according to the observation points, for the levels. At high Reynolds number, this radiation is broadband with significant components for high frequencies, for instance for $St > 1$ in Figure 12, and it is poorly azimuthally correlated. However as the Reynolds number is reduced, the amplitude of this radiation decreases dramatically, the spectra become narrower with a peak moving to lower Strouhal numbers, and the correlation is enhanced. To go further, it can be inferred from the present simulations that this radiation tends to vanish at very low Reynolds number, as vortical structures disappear. The sound source responsible for this broadband radiation is therefore naturally the turbulence developing in the jet itself, corresponding to the so-called fine-scale turbulence in Tam's works.[5,27] Fine-scale turbulence in this jet noise context refers to large and small vortical structures interacting randomly between each others. This sound source may be particularly active in the jet shear layer, where vortices evolve rapidly through catastrophic events, such as pairing or tearing.[15,28] Transition to turbulence in the mixing regions may thus contribute largely to the broadband noise as supported by recent simulations at high Reynolds number where a correlation between the peaks of turbulence intensities in the shear layer and the sound levels in the sideline direction was found.[17]

A second source generating a low-frequency radiation predominant in the downstream direction is clearly observed. Unlike the first source, the radiation generated by this source is not very sensitive to Reynolds number effects. At all Reynolds numbers indeed, spectra at the downstream observation point are dominated by well-marked peaks at Strouhal number $St \simeq 0.25$ with rather close levels. Moreover, the azimuthal correlations are high and do not vary appreciably with Reynolds number. An other difference with the noise radiated by the first source is the scaling with velocity of the peak levels, which follow a u_j^9 power law at the downstream observation point of the present study. This radiation is also highly directional since the is no evidence of its possible contribution to the spectra at the sideline observation point even when the fine-scale turbulence noise is dramatically reduced at the lower Reynolds number $\mathrm{Re}_D = 1700$. This is illustrated in Figure 16 where the Strouhal number peaks obtained both in the downstream and sideline directions are plotted as a function of Reynolds number: the Strouhal peak in the sideline direction decreases regularly at lower Reynolds and does not degenerate to the typical $St \simeq 0.25$ found downstream. Note also that, in addition to be poorly affected by changes in Reynolds number, the downstream low-frequency noise was shown in simulations at high Reynolds number[17] not to very depend on the inflow conditions, and therefore on the development of the turbulence in the shear layer The second jet noise source is thus nearly independent from the jet turbulence and must be only connected to the very large structures of the jet. In the same way as in Tam's theory,[5] very large structures here refer to structures typically of the size of the jet radius or/and instability waves growing in the shear layer. The basic mechanism of this second sound source is indeed still discussed. The rapid growth and decay of instability waves in the shear layer was for instance proposed,[29] and it is interesting to notice that it is likely to

generate a highly directional radiation. The intrusion of vortical structures in the potential core, occurring periodically at a frequency corresponding to the downstream sound frequency, was also suggested by a first simulation of the authors.[15] This mechanism should be subsequently tracked in the present simulations with varying jet parameters. To advance the understanding of subsonic jet noise, the nature of the fondamental jet instability providing the fixed frequency peak of the downstream radiation is also to be investigated theoretically.

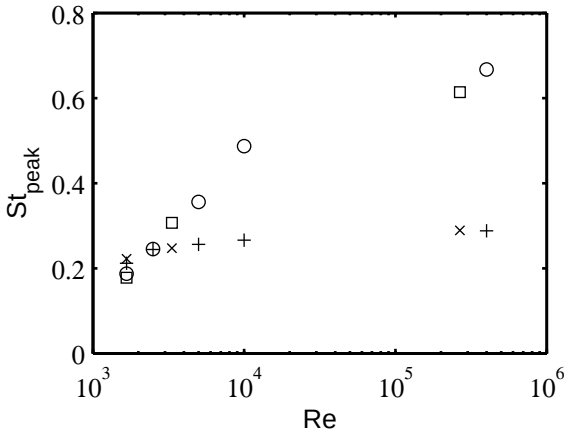

Figure 16: Scaling with Reynolds number of the peak Strouhal numbers obtained in the downstream direction for the + Mach 0.9 and × Mach 0.6 jets, and in the sideline direction for the o Mach 0.9 and □ Mach 0.6 jets.

V. Conclusion

In the present paper, the sound fields generated by subsonic jets at different Mach and Reynolds numbers have been calculated directly by Large Eddy Simulation, and compared to investigate the properties of jet noise sources. The following conclusions were reached.

Two distinct radiations are observed. The first one dominates for large angles from the jet direction but can also be found in the downstream direction. It is is broadband and poorly azimuthally correlated. The second radiation dominates for shallow angles but is negligible for large angles. It appears as a low-frequency peak at a fixed Strouhal number and is highly azimuthally correlated. As the jet velocity varies, spectra of both radiations are seen to scale in frequency with Strouhal number. The scalings of levels however differ: the levels of the first radiation follow a power law of about $u_j^{7.5}$ and those of the second radiation a power law u_j^9. As the Reynolds number decreases, the levels of the first radiation are significantly lower and a large high-frequency part of the sound spectra disappears, whereas the properties of the second radiation do not change significantly. These observations support the theory of two basic components in subsonic jet noise: one, responsible for the broadband radiation, connected to the fine-scale turbulence, and an other, radiating downstream, associated to very large structures of the jet and/or instability waves.

Finally let us draw the reader's attention to the difficulties of Large Eddy Simulation for computing jet noise with fidelity. Since numerical and modelling limitations and errors affect mainly the fine-scale structures, one can expect the low-frequency downstream noise, nearly independent from the jet turbulence, to be well reproduced, but also the calculation of the broadband noise to be especially tricky. In particular, since the fine-scale noise was shown to spectacularly vary according to the Reynolds number, subgrid modellings such as those based on dissipative schemes or on a turbulent viscosity, which might artificially decrease the effective flow Reynolds number,[18] are not to be recommended.

Acknowledgments

This work is supported by the french network RRIT "Recherche Aéronautique sur le Supersonique" (Ministère de la Recherche). Computing time is supplied by the Institut du Développement et des Ressources en Informatique Scientifique (IDRIS - CNRS).

References

[1]Tam, C.K.W., 1995, Supersonic jet noise, *Annu. Rev. Fluid Mech.*, 17-43.

[2]Tam, C.K.W., 1998, Jet noise: since 1952, *Theoret. Comput. Fluid Dynamics*, **10**, 393-405.

[3]Lilley, G.M., 1994, Jet noise classical theory and experiments, *Aeroacoustics of flight vehicles Vol. 1: noise sources*, edited by H.H. Hubbard, 211-289.

[4]Mollo-Christensen, E., Kolpin, M.A. & Martucelli, J.R., 1964, Experiments on jet flows and jet noise far-field spectra and directivity patterns, *J. Fluid Mech.*, **18**, 285-301.

[5]Tam, C.K.W., Golebiowski, M. & Seiner, J.M., 1996, On the two components of turbulent mixing noise from supersonic jets, AIAA Paper 96-1716.

[6]Viswanathan, K., 2003, Jet aeroacoustic testing: issues and implications, *AIAA Journal*, **41**(9), 1674-1689.

[7]Zaman, K.B.M.Q. & Yu, J.C., 1985, Power spectral density of subsonic jet noise, *J. Sound Vib.* **98**(4), 519-537.

[8]Lush, P.A., 1971, Measurements of subsonic jet noise and comparison with theory, *J. Fluid Mech.*, **46**(3), 477-500.

[9]Ahuja, K.K., 1973, Correlation and prediction of jet noise, *J. Sound Vib.* **29**(2), 155-168.

[10]Tanna, H.K., 1977, An experimental study of jet noise. Part I: Turbulent mixing noise. *J. Sound Vib.*, **50**(3), 405-428.

[11]Crighton, D.G., 1981, Acoustics as a branch of fluid mechanics, *J. Fluid Mech.*, **106**, 261-298.

[12]Stromberg, J.L., McLaughlin, D.K. & Troutt, T.R., 1980, Flow field and acoustic properties of a Mach number 0.9 jet, at a low Reynolds number. *J. Sound. Vib.*, **72**(2), 159-176.

[13]Long, D.F. & Arndt, R.E.A, 1984, Jet noise at low Reynolds number, *AIAA Journal*, **22**(2), 187-193.

[14]Freund, J.B., 2001, Noise sources in a low-Reynolds-number turbulent jet at Mach 0.9, *J. Fluid Mech.*, **438**, 277-305.

[15]Bogey, C., Bailly, C. & Juvé, D., 2003, Noise investigation of a high subsonic, moderate Reynolds number jet using a compressible LES, *Theoret. Comput. Fluid Dynamics*, **16**(4), 273-297.

[16]Bogey, C. & Bailly, C., 2002, Direct computation of the sound radiated by a high Reynolds number, subsonic round jet *CEAS Workshop From CFD to CAA*, 2002, Athens, Greece.

[17]Bogey, C. & Bailly, C., 2003, LES of a high Reynolds, high subsonic jet : effects of the inflow conditions on flow and noise, *9th AIAA/CEAS Aeroacoustics Conference*, AIAA Paper 2003-3170.

[18]Bogey, C. & Bailly, C., 2003, LES of a high Reynolds, high subsonic jet : effects of the subgrid modellings on flow and noise, *16th AIAA Computational Fluid Dynamics Conference*, AIAA Paper 2003-3557.

[19]Bogey, C. & Bailly, C., 2004, A family of low dispersive and low dissipative explicit schemes for flow and noise computations, *J. Comput. Phys.*, **194**(1), 194-214.

[20]Visbal, M.R. & Rizzetta, D.P., 2002, Large-Eddy Simulation on curvilinear grids using compact differencing and filtering schemes, *J. Fluids Eng.*, **124**, 836-847.

[21]Bogey, C. & Bailly, C., 2002, Three-dimensional non reflective boundary conditions for acoustic simulations: far-field formulation and validation test cases, *Acta Acustica*, **88**(4), 463-471.

[22]Michalke, A., 1984, Survey on jet instability theory, *Prog. Aerospace Sci.*, **21**, 159-199.

[23]Lau, J.C., 1981, Effects of exit Mach number and temperature on mean-flow and turbulence characteristics in round jets, *J. Fluid Mech.*, **105**, 193-218.

[24]Maestrello, L., 1976, Two points correlations of sound pressure in the far field of a jet: Experiment, NASA-TMX-72835.

[25]Juvé, D., Sunyach, M. & Comte-Bellot, G., 1979, Filtered azimuthal correlations in the acoustic far field of a subsonic jet, *AIAA Journal*, **17**(1), 112-113.

[26]Juvé, D. & Sunyach, M., 1978, Structure azimutale du champ acoustique lointain d'un jet subsonique, *C. R. Acad. Sc. Paris*, t. 287, série B, 187-90 (in french).

[27]Tam, C.K.W. & Auriault, L., 1999, Jet mixing noise from fine-scale turbulence, *AIAA Journal*, **37**(2), 145-155.

[28]Hileman, J. & Samimy, M., 2001, Turbulence structures and the acoustic far field of a Mach 1.3 jet, *AIAA Journal*, **39**(9), 1716-1727.

[29]Huerre, P. & Crighton, D.G., 1983, Sound generation by instability waves in a low Mach number jet, AIAA Paper 83-0661.